Catalysis
Science & Technology

RSC Publishing

PAPER

View Article Online
View Journal | View Issue

Cite this: *Catal. Sci. Technol.*, 2013, **3**, 1017

Synthesis of mesoporous bimetallic Ni–Cu catalysts supported over ZrO_2 by a homogenous urea coprecipitation method for catalytic steam reforming of ethanol

Pankaj Kumar Sharma, Navin Saxena, Arti Bhatt, Chitra Rajagopal and Prasun Kumar Roy*

The synthesis of mesoporous Ni–Cu bimetallic oxides supported over ZrO_2 by the homogenous urea co-precipitation technique and its catalytic efficacy towards steam reforming of ethanol has been explored. The amount of NiO was kept constant and that of CuO was varied to obtain bimetallic supported oxides which were characterized using different techniques like N_2 adsorption–desorption measurements, XRD, H_2-TPR, ICP-OES, TGA and SEM analyses. The results were compared with those obtained by alkali coprecipitation. The oxides prepared by urea coprecipitation were found to exhibit a type IV isotherm and a characteristic H2 type hysteresis, while those prepared by alkali precipitation were found to be nonporous. The studies reveal that this facile route of urea-coprecipitation can generate mesoporosity in zirconia based compositions and because of its simplicity, it holds enormous potential as a soft-templating technique for large scale preparation. The surface area increased on introduction of Cu, exhibits maxima at 3% w/w CuO, and subsequently decrease at higher loadings. The reducibility and the metal support interactions were altered in the presence of Cu, which reflected on its improved catalytic activity towards steam reforming of ethanol. The introduction of Cu species enhances the water gas shift reaction and favors acetaldehyde decomposition and reforming over the ethanol dehydrogenation reaction, as indicated by the reduced levels of acetaldehyde in the product stream. On increasing the reforming temperature, H_2 and CO_2 selectivity and ethanol conversion increased significantly. Bimetallic oxides containing 3% w/w CuO were found to be most effective towards ethanol steam reforming, exhibiting complete ethanol conversion and 84% H_2 selectivity at 600 °C, indicating their potential to be used as stable ESR catalysts.

Received 10th August 2012,
Accepted 10th December 2012

DOI: 10.1039/c2cy20563g

www.rsc.org/catalysis

1. Introduction

Mesoporous materials hold enormous potential in diverse fields especially catalysis, adsorption, separation by molecular sieving, sensing and environment management.[1] Their synthesis generally relies on the hydrolysis of alkoxides to form a network on a soft template (supramolecular assembly of surfactants or block copolymers) or hard template (porous alumina, silica, carbon, polymer), which is subsequently removed.[2,3] Lately, synthetic approaches involving the use of non-surfactant organic compounds like D-glucose, dibenzoyl-L-tartaric acid and urea have also been attempted.[4]

In the search of catalytically active mesoporous materials, numerous efforts have been directed towards the synthesis of non-siliceous materials, as they offer promise as high surface area substrates.[5,6] However, these materials are relatively difficult to prepare by application of principles common to synthesis of silica-based networks, because of the former's susceptibility towards redox reactions, hydrolysis or phase transformations. Moreover, techniques which have proven successful for template removal in siliceous materials *e.g.* calcination, solvent extraction and UV-ozone treatment *etc*. are not so successful in the preparation of non-siliceous counterparts, as these are more susceptible to collapse. These critical issues, particularly with respect to the high cost and tedious processing, pose hindrance to the large scale production and application of mesoporous materials.[3]

One such non-siliceous material, ZrO_2, has been extensively studied because of its high chemical stability, acidic–basic surface

Centre for Fire, Explosive and Environment Safety, Brig. S. K. Majumdar Marg, Delhi 110054, India. E-mail: pk_roy2000@yahoo.com; Fax: +91-11-23819547; Tel: +91-11-23907191

containing hydroxyl moieties[7] along with unique redox properties,[8] which are useful characteristics for catalyzing reactions which suffer from deactivation due to carbon formation. Ethanol steam reforming (ESR) is one such reaction and since the organic feed required for this purpose can be obtained by fermentation of biomass, this reaction has a great potential for hydrogen generation by a practically closed carbon cycle, resulting in a positive impact on the environment at large.[9,10] Numerous efforts are being directed towards development of catalysts which can render this reaction practical for large scale hydrogen production.[11]

Density functional theoretical calculations reveal that the most active metal species for catalyzing ESR include Ni, Ir, Rh and Co, which basically reduce the C–H, C–C and C–O dissociation barriers.[12] Due to economic factors, nickel is most commonly employed, however it is susceptible to deactivation due to coke formation.[13] Our hypothesis is that the use of mesoporous substrates loaded with these active species can further improve the catalytic performance and recent studies on nickel supported over mesoporous ceria–zirconia have proven the same.[14]

To improve the activity of nickel based catalysts towards ESR, we have attempted to design bimetallic oxides with copper as the second component as Cu has been reported to be an efficient catalyst for the water gas shift reaction[15] and a strong inhibitor towards coke formation.[16] Preparation of such bimetallic supported catalysts is by no means a new research topic and several groups are investigating bimetallic systems for reforming varied feedstocks including higher hydrocarbons for the generation of hydrogen.[17,18]

This article deals with the preparation of mesoporous bimetallic zirconia based catalysts, using the urea coprecipitation technique. The simplicity of this route makes it a practicable choice for large scale production of similar materials, as template removal is straightforward. The application of the oxide towards catalytic ESR has also been studied to quantify the effects of introduction of Cu on the overall performance of the catalyst.

2. Experimental procedures

2.1. Materials

Metal precursors in the form of respective nitrates (*viz.* $Ni(NO_3)_2{\cdot}6H_2O$, $Cu(NO_3)_2{\cdot}3H_2O$ and $ZrO(NO_3)_2{\cdot}xH_2O$), urea and ethanol were purchased from E. Merck (Germany) and were used without any further purification. Double distilled water was used throughout the course of the experimental work.

2.2. Synthesis of mesoporous oxides

A series of Ni–Cu bimetallic catalysts, supported over ZrO_2, was prepared by a homogeneous urea co-precipitation method. The amount of NiO was kept constant at 25% w/w throughout, and that of ZrO_2 was varied depending on the amount of CuO required in the final composition *i.e.*, 3, 5, 7 and 9% w/w. In brief, required quantities of nitrates of constituent metals were dissolved in double distilled water and reacted with stoichiometric quantity of urea. The resulting homogenous solution was refluxed for ~48 h under constant stirring and the pH of the medium was monitored at time intervals of 4 h till no further increase in pH was observed. The resulting coarse precipitates were washed thoroughly, dried in an air oven at 90 °C for 12 h and subsequently calcined in a muffle furnace at 550 °C for 6 h. These samples have been referred to as NCZ-*x* (where N, C and Z refer to nickel, copper and zirconium and *x* = 3, 5, 7 and 9 stand for the desired weight% of CuO) in the text, subsequently. Similarly, monometallic NiO (25% w/w) and CuO (25% w/w) supported on ZrO_2 were also synthesized by the same technique, which have been referred to as NZ and CZ, respectively. Hydroxides of Ni, Cu and Zr separately were also precipitated by the same method for investigating their thermal behavior. For comparison purposes, the entire series of oxides were prepared by a conventional coprecipitation route, using sodium hydroxide as the precipitant. Aqueous NaOH (1 M) solution was added dropwise to the aqueous metal nitrate solution (1 M) under constant stirring at 60 °C till the pH reached ~10. The precipitate obtained was allowed to age for 24 h, filtered, washed repeatedly with water, dried and calcined under the same conditions (550 °C, 6 h). The samples have been referred to as NCZCp-*x* (where N, C and Z refer to nickel, copper and zirconium and *x* = 3, 5, 7 and 9 stand for the desired weight% of CuO).

2.3. Characterization of catalysts

The chemical composition was determined by acid digestion of the samples using a JSGW Kjeldahl Digesdahl apparatus. In brief, the sample (~0.5 g) was digested in conc. HNO_3 (10 mL) for extended periods, followed by quantification of the metal concentration using an Inductive Coupled Plasma–Optical Emission Spectrometer (Perkin Elmer Optima 2100 DV). The thermal behavior of the precursors was studied using a Perkin Elmer simultaneous TG/DTA instrument (Diamond SDTA), for which the samples were subjected to a temperature program from 50 °C to 600 °C, under an air atmosphere at a heating rate of 10 °C min^{-1}. The textural properties of the calcined samples were studied by a N_2 adsorption–desorption study on a Surface Area Analyzer (Micromeritics ASAP 2010). For this purpose, the samples were initially degassed under vacuum at 100 °C for 16 h and the nitrogen adsorption–desorption experiments were performed at 77 K. The identification of crystalline phases in the sample was performed by powder X-ray Diffraction (XRD) analysis on a Philips PANalytical 1730 diffractometer using Cu K_α (λ = 1.54 Å) where the diffractograms were recorded over a range of $2\theta = 20^\circ$ to 60°.

The reduction behavior of oxides was studied by temperature programmed reduction (TPR) and the active metal surface area measurements using CO chemisorption performed on a Chemisorption analyser (Micromeritics Chemisorb 2920). For the purpose of TPR, 17 mg of the sample was subjected to a temperature program from 30 °C to 600 °C at a heating rate of 10 °C min^{-1} under a hydrogen atmosphere (flow rate 25 ml min^{-1}). For pulse chemisorption, approximately 500 mg of catalyst was first equilibrated at 120 °C for 2 h to drive out volatiles and subsequently the temperature was raised to 400 °C in the presence of H_2–Ar (10% v/v) for 3 h to ensure complete reduction. Purging was performed under flowing He for 1 h after which the

sample was cooled to 50 °C. Chemisorption experiments were performed with a CO–helium mixture (10.5% v/v), where a pulse was introduced after each 2 min interval till the area of successive hydrogen peaks was found to be identical. Temperature programmed oxidation studies on the catalyst samples post-reforming experiments were carried out to determine the amount and type of coke deposited. For this purpose, the sample was heated at 10 °C min^{-1} in 10 ml min^{-1} flow of O_2–He (10% v/v).

The surface morphology of the samples was examined by field emission scanning electron microscopy. Sample surfaces were sputtered with gold using usual techniques and then analysed in FE SEM (SUPRA 55, Carl Zeiss) using a voltage of 15 kV. Photo-micrographs were taken at a uniform magnification of $\sim$50 000×.

2.4. Catalytic evaluation

Catalytic steam reforming of ethanol was performed on a packed bed down flow vertical tubular stainless steel reactor (18 mm dia × 38 mm length) at atmospheric pressure. 1 g of the sample was loaded into the reactor and reduced under continuous H_2 flow (200 ml min^{-1}), while maintaining the temperature of 500 °C for a period of 6 h prior to performing the reforming experiments.

The reforming studies were conducted on an aqueous solution of ethanol, where the water to ethanol molar ratio was preset at 6 : 1. The liquid was fed by a peristaltic pump at a flow rate of 1 ml min^{-1}, corresponding to a W/F_{A0} of 6×10^{-2} h, into an external preheater unit, which was maintained at 300 °C for gasification of the inlet stream. The ethanol–steam mixture was then fed to the reactor unit where the temperature was varied (400 °C–700 °C). The outlet stream consisting of products and unconverted species was made to pass through a condenser maintained at 4 °C and a liquid–gas separator followed by sampling ports. The reaction products were analyzed by a CIC-WIN online gas chromatograph, equipped with a thermal conductivity detector (TCD) and porapak-Q column and a molecular sieve 5A column for the gaseous product concentration measurement. The concentration of species present in the liquid condensate was measured by a Flame Ionization Detector (FID), where the separation of the constituents was performed on a chromosorb column. The response factors for all species were calculated, and the system was calibrated with appropriate standards before each sample run.

To evaluate the catalyst performance, ethanol conversion (X_{EtOH}) and selectivity to hydrogen (S_{H2}) and carbon containing species (S_x) were determined as follows

$$X_{EtOH} = \frac{\text{Moles}_{EtOH(in)} - \text{Moles}_{EtOH(out)}}{\text{Moles}_{EtOH(in)}} \times 100$$

$$S_{H_2} = \frac{\text{Moles of } H_2 \text{ produced}}{\text{Total moles of hydrogen in products}} \times 100$$

$$S_x = \frac{\text{Moles of carbon in product X}}{\text{Total moles of carbon in gaseous and liquid products}} \times 100$$

3. Results and discussion

Mesoporous bimetallic oxides of nickel and copper supported over zirconia were prepared by the homogenous urea co-precipitation technique and its catalytic performance towards ESR was investigated as a function of temperature in a fixed bed configuration. The effect of incorporation of copper in the formulation on the catalytic activity is also discussed.

3.1. Mesoporous nature of bimetallic supported oxides

The nitrogen adsorption–desorption isotherms of the oxides, prepared by the urea hydrolytic decomposition process, are presented in Fig. 1. For comparison purposes, the isotherms of the samples prepared by the sodium hydroxide aided co-precipitation route are also presented. As is apparent, the samples obtained by alkali precipitation were non-porous in nature, while those prepared by urea decomposition exhibit a hysteretic behaviour (type H2), which confirm its mesoporous nature. The initial part of the isotherm is a result of the monolayer–multilayer adsorption, and the hysteretic loop is associated with capillary condensation occurring within the mesopores. The mechanism behind the generation of mesoporosity using a non-surfactant templating pathway has not been fully explicated and is a topic of much research interest. Recently, the synthesis of a similar mesoporous non-siliceous titania–silica substrate has been reported by the acid catalysed hydrolysis of tetrabutyl titanate and tetraethyl orthosilicate in the presence of urea as a soft template.[19] However, under the reaction conditions employed during the sol–gel process, the role of urea is restricted to that of a porogen. In the present case, mesoporosity in the samples is generated even when urea is present only in stoichiometric amounts. The hydrolytic decomposition of urea is reportedly slow under ambient conditions,[20] and raising the temperature accelerates this reaction, thereby leading to the formation of carbon dioxide and ammonia as shown below.[21]

$$NH_2CONH_2 + H_2O \rightarrow CO_2 + 2NH_3$$

$$2NH_3 + H_2O \rightarrow 2NH_4^+ + 2OH^-$$

$$M^{n+} + nOH^- \rightarrow M(OH)_n$$

$$M(OH)_n \cdot xH_2O \rightarrow \text{M-Oxide}$$

In the initial stages of the reaction, urea primarily plays a templating role, since no other substrate is present. With time, urea hydrolyses, resulting in the formation of micrometer sized CO_2 bubbles and NH_3. The generation of NH_3 brings forth a steady increase in the pH of the solution, which finally leads to the precipitation of the metals in the form of hydroxides. The increase in pH as a function of hydrolysis duration for three representative samples is presented in Fig. 2. The freshly crystalline nanoparticles have a tendency to aggregate around the gas/liquid interface of CO_2 and water, a process which is driven by the minimization of interfacial energy. With the progress of the reaction, the walls of the hollow spheres

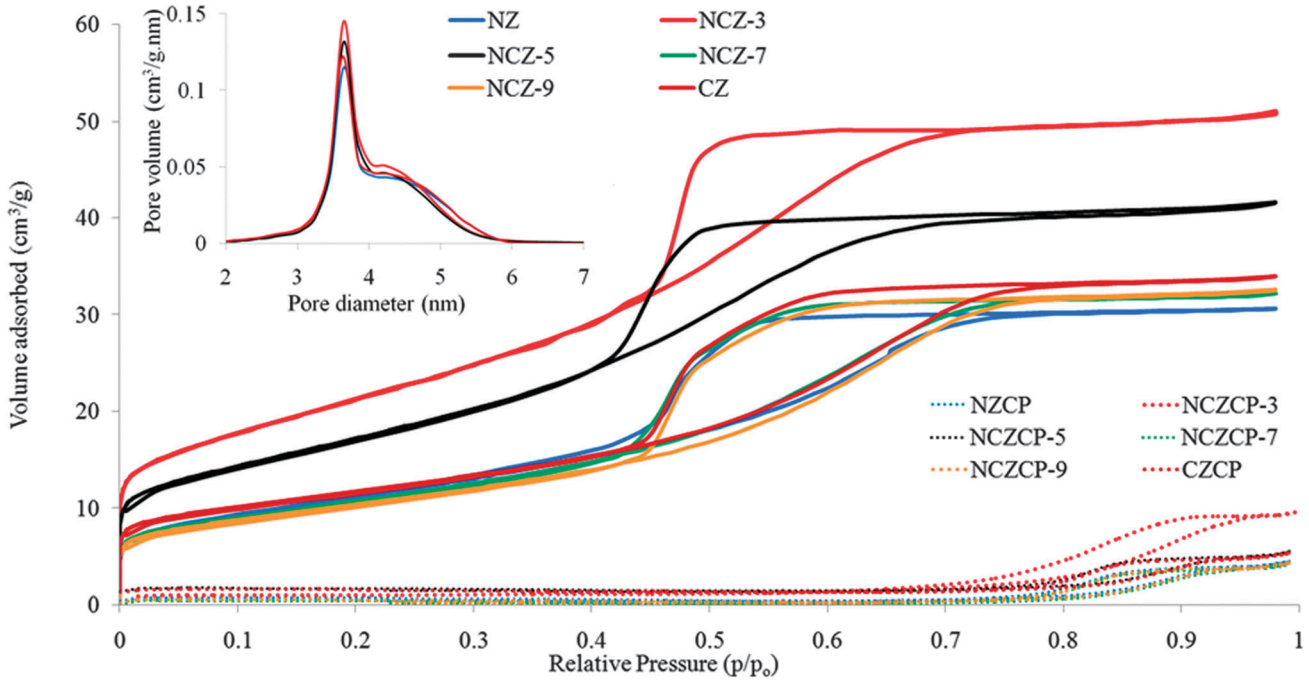

Fig. 1 Nitrogen adsorption–desorption isotherms of calcined oxides. Inset shows the pore size distribution obtained from the BJH desorption curve.

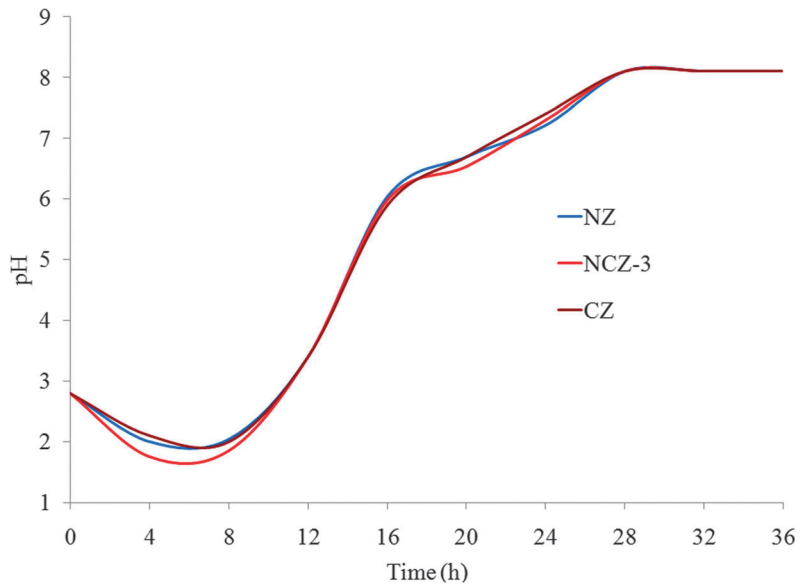

Fig. 2 Increase in pH due to hydrolytic decomposition of urea.

become thicker at the expense of the particle dissolution, typical of an Ostwald process.[22]

The Barrett–Joyner–Halenda (BJH) method was used to determine the pore size distribution from the desorption branch of the isotherms (inset, Fig. 1). It can be seen that all the samples possess pores with diameters ranging from 2.5–6 nm. As reported previously,[23] urea hydrolysis led to the precipitation of samples in the form of coarse powders, the formation of which is attributed to high temperature and low supersaturation preparation conditions. The BET surface areas of the oxides prepared by the urea coprecipitation route are presented in Table 1. NZ was found to exhibit a surface area of 41.2 $m^2\ g^{-1}$ and introduction of small amounts of copper oxide (3% w/w) leads to a substantial enhancement in the surface area which may be attributed to the ability of the second component to increase the dispersion of nickel on the surface of ZrO_2. However, as the concentration of Cu was increased further, the surface area was adversely affected, but was higher than NZ. On the other hand, when the oxides were prepared by the conventional co-precipitation route using

Table 1 Chemical composition and surface properties of the NCZ-*x* catalysts

S. No	Catalyst	Weight% of metals Experimental (theoretical) Ni	Cu	Zr	ZrO_2 crystallite size (nm)	NiO crystallite size (nm)	BET surface area ($m^2\ g^{-1}$)
1	NZ	11.18 (13.21)	— 0	63.76 (61.58)	9.8	19.5	41.2
2	NCZ-3	10.5 (13.37)	3.51 (1.74)	67.32 (59.83)	8.4	14.4	77.6
3	NCZ-5	11.3 (13.48)	5.24 (2.92)	68.81 (58.63)	8.4	14.3	63.8
4	NCZ-7	16.9 (19.59)	6.64 (4.12)	68.63 (57.42)	8.1	13.1	39.4
5	NCZ-9	11.51 (13.7)	7.24 (5.33)	68.61 (56.18)	8.3	13.8	37.3
6	CZ	— 0	13.98 (14.14)	61.23 (60.92)	7.69	—	39.2

sodium hydroxide precipitant, the samples exhibited very low surface areas (1–2 $m^2\ g^{-1}$). This can be explained on the basis of instantaneous pH differences that lead to local supersaturation in different parts of the slurry.[16] Since the efficiency of any catalyst is primarily dependent on its surface area, which was found to be an order of magnitude higher for urea-coprecipitated oxides, further characterization and catalytic studies have been performed on the NCZ-*x* series.

3.2. Physico-chemical properties

The elemental composition of the calcined oxides was determined by digesting the samples in acidic medium followed by analysis using Inductively Coupled Plasma–Optical Emission Spectroscopy (ICP-OES) and the results are presented in Table 1. It can be seen that the experimentally determined results differ from the theoretically estimated figures, which were calculated assuming complete conversion of constituent metal nitrates into oxides, post-calcination. Speciation studies indicate that copper ceases to exist in its soluble ionic state at pH 6, but a much higher hydroxide ion concentration is required to precipitate nickel as it hydroxide, which starts at pH 8.[24,25] On the other hand, zirconium has been reported to exist as neutral species $[Zr(OH)_4]_{aq}$, at much reduced acid concentrations[26] and complete precipitation as hydroxide has been reportedly achieved by the urea hydrolysis technique previously.[27] Based on the above, it can be concluded that since the pH achieved by hydrolysis of urea is limited to a maximum of 8, the reaction medium does not seem to possess the requisite basicity to precipitate nickel in its entirety, but almost complete precipitation of the other two constituent ions can be achieved. Another reason for this deviation between predicted and experimental values stems from the possibility of formation of mixed oxides, the quantification of which was beyond the scope of the present study.

TG traces of urea, hydroxides of Cu, Ni, Zr and a representative catalyst precursor (NCZ-3) are presented in Fig. 3. Urea, as expected, exhibits a double step decomposition, which results from the sequential decomposition of NH_2CONH_2 reactions (*viz.* $NH_2CONH_2 \rightarrow NH_3 + HNCO$ and $HNCO + H_2O \rightarrow NH_3 + CO_2$) occurring at temperatures 150 °C and 270 °C, respectively.[23] On the other hand, the TG traces of metal hydroxides indicate that nickel and copper hydroxides exhibit sharp single step decomposition, while the decomposition of zirconium hydroxide occurs over a broad range due to the oxidative cleavage of different types of Zr–O bonds present in the hydroxide. In general, the decomposition temperatures of the hydroxides follow the order: copper < nickel < zirconium. The initial mass loss in the TG trace of zirconium hydroxide (<200 °C) is due to the loss of loosely bound water, followed by the water of crystallization, and finally, the decomposition of hydroxides to their corresponding oxides. The TG trace of the representative

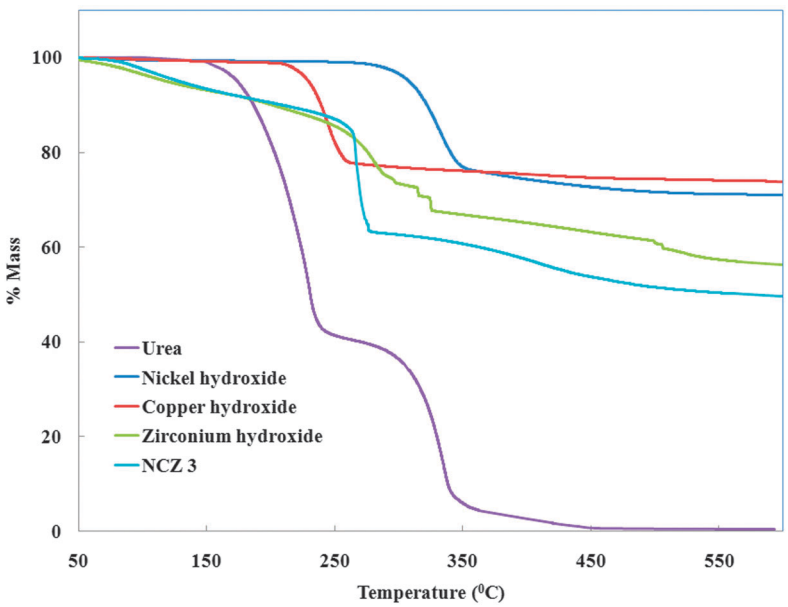

Fig. 3 TG traces of urea, hydroxides of Cu, Ni, Zr and catalyst precursor NCZ-3.

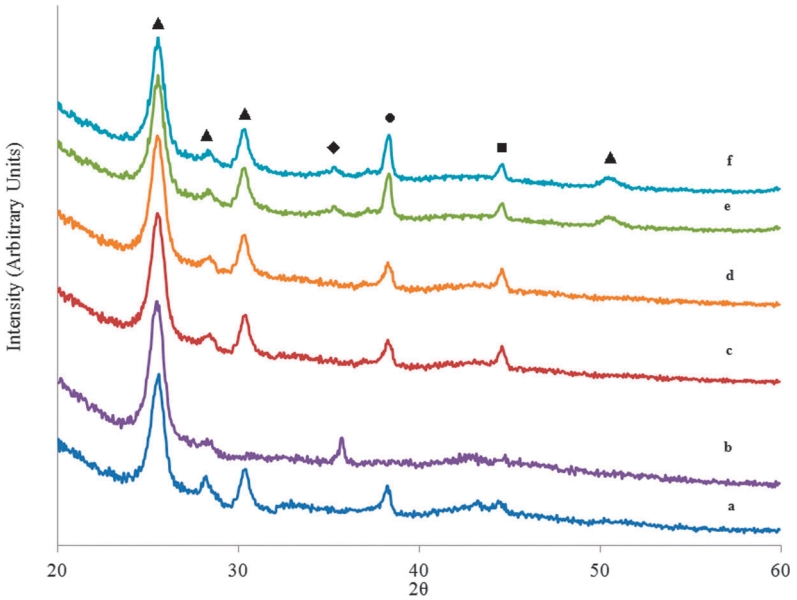

Fig. 4 Powder XRD of calcined oxides: (a) NZ; (b) CZ; (c) NCZ-3; (d) NCZ-5; (e) NCZ-7; (f) NCZ-9 (▲)ZrO_2, (■) Zr_4Ni_2O, (●) NiO, (◆) Cu_4O_3.

catalyst precursor (NCZ-3) is similar to that of zirconium hydroxide except for a sharp mass loss corresponding to the conversion of Ni and Cu hydroxides to their oxides. Since no further loss in mass is observed after 550 °C in the precursor, this was chosen as the suitable temperature for performing calcination to prevent agglomeration at higher temperatures.

The XRD patterns of the calcined samples are shown in Fig. 4. It can be seen that both the tetragonal and monoclinic ZrO_2 phases were present in the calcined samples. A diffraction peak at $2\theta = 24.5^\circ$, characteristic of the (110) plane of tetragonal ZrO_2 (JCPDS 81-1320) and weak peaks corresponding to tetragonal (101) and (112) planes were observed at $2\theta = 30.2^\circ$ and 50.3° respectively (JCPDS 88-1007). In addition, a diffraction peak at 28.1°, corresponding to the (111) plane of monoclinic ZrO_2 (JCPDS 72-1669) was also observed. In nickel containing samples, an additional peak was observed at 44.5° which can be due to the (442) plane of the cubic Zr_4Ni_2O phase (JCPDS 82-0944). Also, the intensity corresponding to the (111) plane of the cubic NiO phase at 37.2° (JCPDS 47-1049) was found to increase with increasing CuO loading in bimetallic samples. In the CZ sample, a peak corresponding to monoclinic Cu_4O_3 at $2\theta = 35.7^\circ$ (JCPDS 49-1830) was observed. However, in bimetallic oxides, at CuO concentrations $\leq 5\%$, this peak could not be seen, which may be attributed to the presence of Cu at a very low concentration or in a highly dispersed state. The average crystallite sizes of different phases present in the prepared catalysts were estimated by the Scherrer equation from the full width at half maximum (FWHM) of corresponding diffraction peaks ($2\theta = 24.5^\circ$ for ZrO_2 and 37.2° for NiO) and are presented in Table 1. It is apparent from the table that there is a decrease in the crystallite size of monoclinic ZrO_2 as well as the cubic NiO phase with the increasing CuO content.

In order to assess the effect of increasing copper content on the reducibility of the samples, temperature programmed

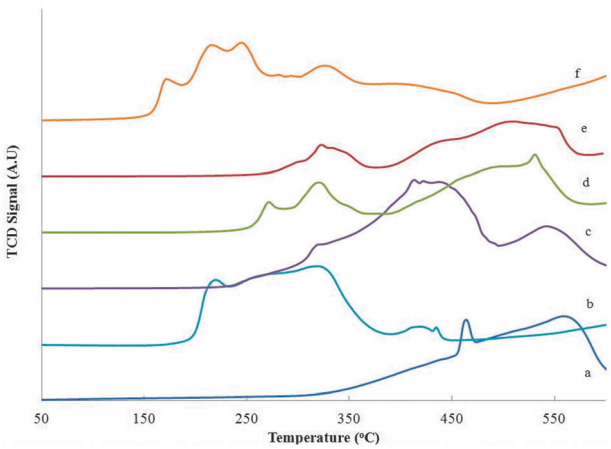

Fig. 5 Temperature programmed reduction profiles of mesoporous oxides: (a) NZ; (b) CZ; (c) NCZ-3; (d) NCZ-5; (e) NCZ-7; (f) NCZ-9.

reduction studies were performed and the results of the same are presented in Fig. 5. ZrO_2 has been reported to be non-reducible by H_2 even under elevated temperatures,[28] thereby indicating that the TCD signals are due to the reduction of the nickel and copper oxide species only. It is apparent from the figure that reduction of CuO → Cu occurs at a much lower temperature as compared to NiO → Ni. However, the reduction of both the species takes place over a broad temperature range, suggesting a wide array of interactions between active metal oxide particles and the support. The prominent peak at ~460 °C in the reduction profile of NZ can be attributed to reduction of surface and free NiO species, with the high temperature peak at ~560 °C resulting from the reduction of bulk NiO. Similarly, in the CZ samples two broad reduction peaks, with the first peak occurring at 200–390 °C, followed by a shoulder peak at ~420 °C were observed. This small shoulder can be attributed to the

Table 2 CO pulse chemisorption results of the NCZ-*x* catalysts

Catalyst	CO uptake (μmol g^{-1})	Dispersion (%)	Active metal surface area (m^2 g^{-1} metal)
NZ	1.87	8.33×10^{-2}	0.55
NCZ-3	11.27	4.43×10^{-1}	2.93
NCZ-5	1.91	8.61×10^{-2}	0.64
NCZ-7	1.08	3.78×10^{-2}	0.21
NCZ-9	1.08	3.40×10^{-2}	0.19

reduction of bulk CuO interacting more strongly with the support as has been reported earlier.[29] The TPR patterns of the bimetallic NCZ-*x* (x = 3, 5, 7, 9) catalysts exhibit reduction peaks corresponding to the temperature of reduction of the constituent oxides of nickel and copper, but the reduction temperature is substantially lowered.

The total CO uptake, % dispersion of active metals and the metallic surface area obtained from CO pulse chemisorption experiments are presented in Table 2. CO chemisorption is reportedly stronger on nickel surfaces than on copper, with the measured heat of adsorption being $\sim$30 kcal mol^{-1} and $\sim$15 kcal mol^{-1} for Ni and Cu respectively.[30] For metallic surface area calculations, the stoichiometric factor of 1 was assumed, which is characteristic of a linear chemisorption conformation (one CO per metal particle).[31]

The results indicate that the total CO uptake, dispersion and metal surface area increased on addition of small amounts of Cu (3% w/w CuO). On increasing the copper loading, the metal dispersion reduced which is expected to reflect on the final catalytic reforming results. The calculated nickel dispersion and nickel surface areas were in the range of 0.03–0.4% and 0.19–2.93 m^2 g^{-1} metal, respectively.

The morphology of the samples was examined using FE-SEM and representative micrographs are presented in Fig. 6. It can be seen that with the introduction of copper in small amounts, the surface of the sample becomes rough, which results in the increased surface area of the sample. With a further increase in the concentration of copper, the surface appears to smoothen out, which also reflected in the lower surface area observed during the N_2 physisorption experiments.

3.3. Catalytic performance of mesoporous oxides towards ESR

Ethanol steam reforming (ESR), being endothermic in nature ($C_2H_5OH + 3H_2O \rightarrow 2CO_2 + 6CO_2$; ΔH°_{298} = 174 kJ mol^{-1}), is favored at high temperatures and low pressures. The effect of

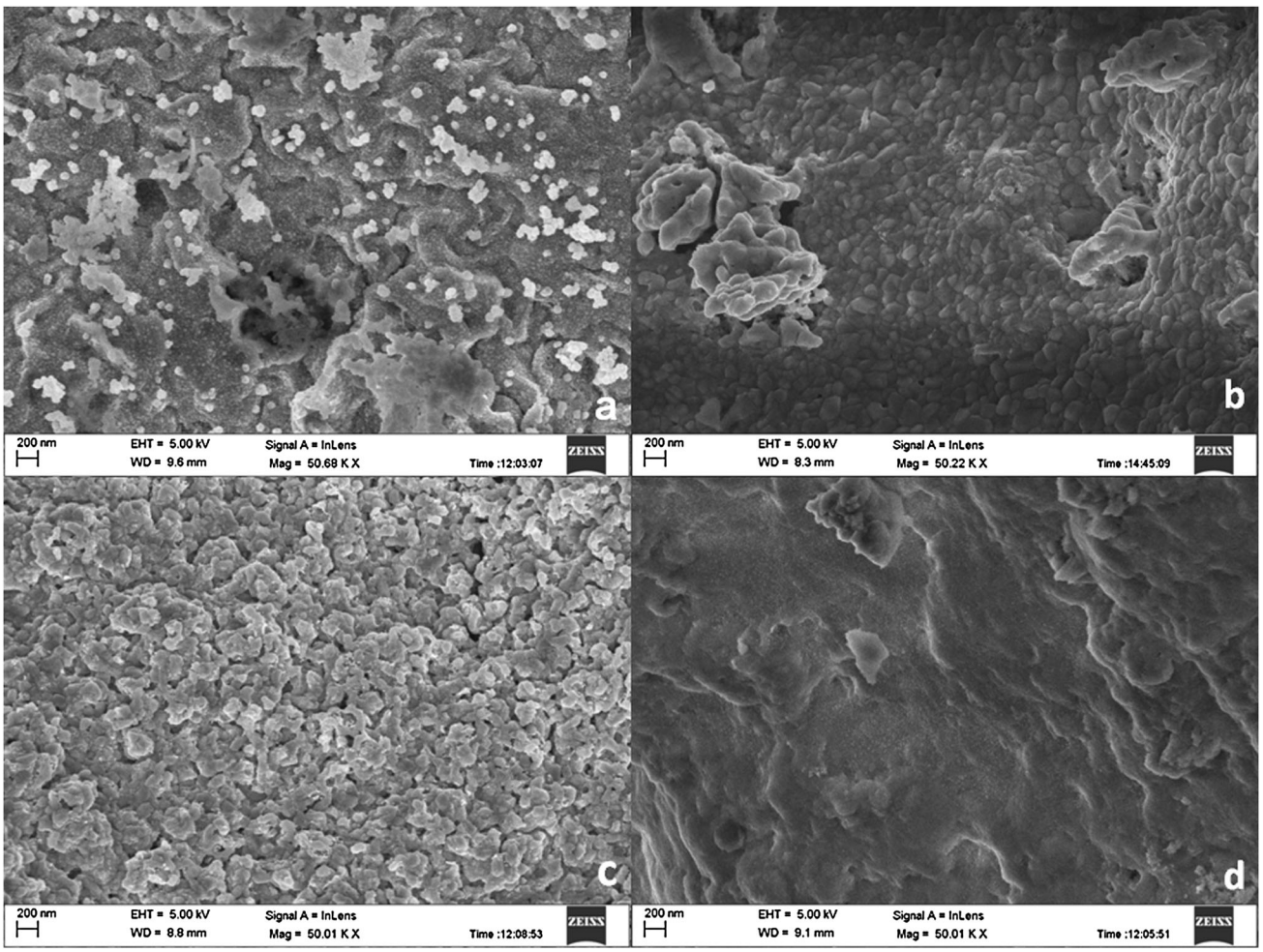

Fig. 6 SEM images of mesoporous oxides: (a) NZ; (b) CZ; (c) NCZ-3; (d) NCZ-9.

operating temperature and amount of copper on the catalytic activity towards ESR was established by performing reforming experiments in a fixed bed reactor at a space velocity of $W/F_{A0} = 6 \times 10^{-2}$ h. The water : ethanol feed ratio was maintained at 6 : 1, as higher amounts of ethanol in the feed have been reported to cause rapid deactivation from coke formation.[32]

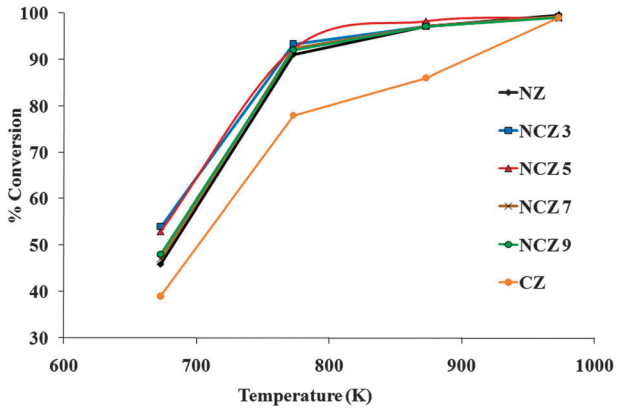

Fig. 7 Effect of temperature and copper concentration on ethanol conversion.

3.3.1. Effect of introduction of copper. The results in terms of conversion and selectivity towards H_2 and other carbonaceous species are presented in Fig. 7 and 8. It can be seen from the figures that the efficiency of the mesoporous catalysts towards ESR increased significantly when small amounts of Cu were present in the composition. Undoped Ni catalyses both ethanol decomposition (ED, $C_2H_5OH \rightarrow CO + CH_4 + H_2$) as well as ethanol reforming, which accounts for the presence of CH_4 and CO in the product stream. Ethanol conversion was considerably low when the experiments were performed at 400 °C, and a significant amount of acetaldehyde was detected in the liquid stream which was attributed to the ethanol dehydrogenation reaction (EDH, $CH_3CH_2OH \rightarrow CH_3CHO + H_2$). On the other hand, in the presence of the CZ catalyst, a substantial amount of ethylene was also detected in the product stream at lower temperatures (Fig. 9), which can be attributed to the strong dehydration ability of copper based catalysts (EDR, $C_2H_5OH \rightarrow H_2O + C_2H_2$).[33–35]

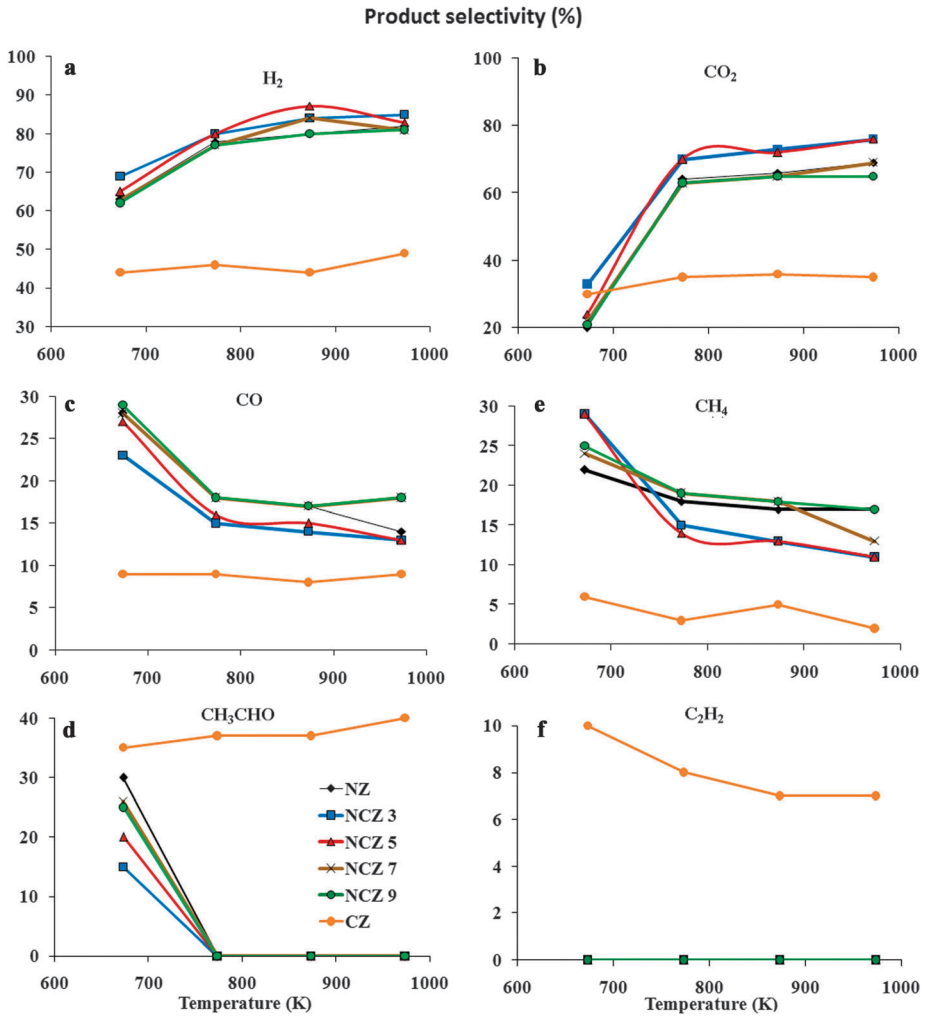

Fig. 8 Effect of temperature and copper concentration on catalytic activity towards steam reforming of ethanol in terms of (a) H_2 selectivity, (b) CO_2 selectivity, (c) CO selectivity, (d) CH_3CHO selectivity, (e) CH_4 selectivity and (f) C_2H_2 selectivity.

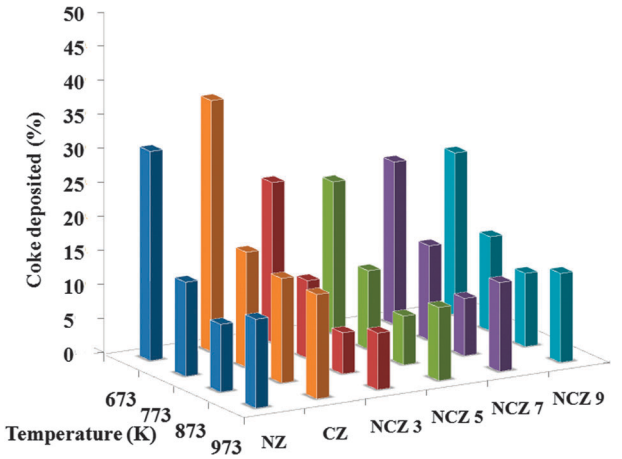

Fig. 9 Reduction in coke due to increase in temperature and copper concentration.

However, for Ni–Cu catalysts, the amount of CH_3CHO and C_2H_2 in the product stream was reduced significantly and at $T > 500$ °C, these could not be detected in the product stream, implying that the rates of ethanol decomposition and acetaldehyde decomposition (AD, $CH_3CHO \rightarrow CH_4 + CO$) are much faster than ethanol dehydrogenation and dehydration. It appears that in the presence of Cu, the CO formed during the reaction further undergoes a water gas shift reaction (WGS, $CO + H_2O \rightarrow CO_2 + H_2$) at rates much faster than ethanol dehydration. The effect of introduction of Cu on the extent of ethanol conversion was more pronounced at lower temperatures (< 500 °C). At 400 °C, the ethanol conversion increased from 43 to 56% by addition of 3 wt% Cu (NCZ-3). For all catalysts, the conversion was >95% at $T \geq 500$ °C. It can be seen that the selectivity towards H_2 and CO_2 increased significantly as the temperature was increased from 400 to 500 °C and was highest for NCZ-3. The selectivity towards CO and CH_4 showed a minimum at ~500 °C after which no further decrease was observed. It appears from our results that at ~500 °C, acetaldehyde decomposition was complete, and the product composition was then controlled by the two reversible reactions of methane steam reforming (MSR, $CH_4 + H_2O \rightarrow CO + 3H_2$) and WGS. Below 500 °C, the rate of WGS is not significant and consequently the selectivity towards CO_2 is low. As the temperature increased to 500 °C, the rates of WGS and MSR become significant resulting in a lower selectivity to CO and CH_4 together with a higher selectivity to H_2 and CO_2. Klouz *et al.*[36] also reported a decrease in the selectivity to CO in the temperature range of 300–400 °C during the ethanol reforming on Ni–Cu/SiO_2. However as the temperature increases further, the reverse WGS ($CO_2 + H_2 \rightarrow CO + H_2O$) and reverse MSR ($CO + 3H_2 \rightarrow CH_4 + H_2O$) reactions also compete towards controlling the product distribution.[37,38]

In the present investigation, the catalyst activity increased with the copper content till a loading of 3% (w/w), but decreased at higher loading. This can be attributed to the higher surface area of the NCZ-3 catalyst. A similar effect of Cu loading of Ni–Cu/Al_2O_3 catalysts has been reported for autothermal reforming of ethanol where a 5 wt% Cu containing catalyst was more active than either a 2% (w/w) or 7% (w/w) Cu containing Ni–Cu catalyst.[39]

Extensive coke formation was observed, especially at low temperatures, the amount of which decreased with increase in reforming temperatures (Fig. 9). The carbon formation during ESR occurs primarily by the dissociation of the hydrocarbon molecule formed during the reaction or the dissociation of CO according to the Boudouard reaction.[11] The extent of coke deposited on the sample was quantified using TPO studies. Two distinct peaks were observed in the TPO profiles of all samples, the peak corresponding to lower temperature (< 300 °C) being attributed to the oxidation of amorphous carbon and the other peak at $T > 600$ °C was ascribed to the oxidation of graphitic carbon. The studies revealed that in all the experiments, the fraction of amorphous carbon deposited on the catalyst was much higher (80 ± 5%), the remnant being graphitic in nature. Interestingly, although the amount of coke formed on the CZ catalyst was higher, it was mainly amorphous in nature (~94%), with a minor graphitic content. In all samples, no significant deactivation occurred due to coke deposition (over 50 h) and the catalyst could be easily regenerated by air oxidation at 600 °C, which suggests their potential as a stable ESR catalyst.

An efficient catalyst for ethanol reforming should be capable of rupturing the C–C bond and should also be active towards water gas shift (WGS). In this context, the activity of Ni towards WGS is low[33–35] and the introduction of copper as a WGS catalyst,[16,39,40] in the catalyst formulation, appears to reduce the level of CO in the product stream. Apart from being an efficient WGS catalyst, Cu also plays an important role in lowering the reduction temperature of Ni species as is evident from the TPR results, which in turn is a result of reduced interaction between the support and the active metal.

4. Conclusion

A facile homogenous urea co-precipitation technique was successfully employed for the preparation of mesoporous Ni–Cu bimetallic oxides supported over ZrO_2. The amount of NiO was fixed at 25% w/w and that of CuO was varied in the range 3–9% w/w. The oxides exhibit a type IV adsorption–desorption isotherm, with a type H2 hysteresis, characteristic of their mesoporous nature, while the same samples when prepared by alkali precipitation were non-porous and exhibited low surface areas (~1–2 $m^2\ g^{-1}$). The active transition metal oxides were reduced to their active state and studied for their ability to catalyze steam reforming of ethanol. Introduction of copper was found to lower the reduction temperature of the catalyst, which results from the increase in dispersion of nickel species indicating the active role of the second component on the alteration of metal support interaction. At lower loadings, copper results in an increased surface area and mesoporosity which reflect on the improved catalytic performance of the material. Water gas shift reaction and acetaldehyde decomposition as well as reforming is favored over ethanol dehydrogenation in the presence of copper, as indicated by the reduced levels of acetaldehyde in the product stream. Bimetallic oxide

containing 3% w/w CuO was found to be the most effective catalyst for the said purpose, exhibiting complete ethanol conversion and 84% H_2 selectivity at 600 °C. The catalyst does not lose its activity over a period of 50 h, indicating its potential to be used as a stable ESR catalyst. The studies indicate that this route of urea-coprecipitation holds enormous potential as a soft-templating technique for large scale preparation of mesoporous support.

Acknowledgements

The authors are thankful to Dr Sudershan Kumar, Director, Centre for Fire, Explosive and Environment Safety, for taking keen interest and for providing the laboratory facilities. Thanks are also due to Dr P. K. Rai, CFEES, for physisorption studies, Dr Ashok Kapoor, SSPL, for XRD and SEM analysis.

References

1 V. Meynen, P. Cool and E. F. Vansant, *Microporous Mesoporous Mater.*, 2009, **125**, 170–223.
2 A. Vinu, T. Mori and K. Ariga, *Sci. Technol. Adv. Mater.*, 2006, **7**, 753–771.
3 U. Ciesla, D. Demuth, R. Leon, P. Petroff, G. Stucky, K. Unger and F. Schuth, *J. Chem. Soc., Chem. Commun.*, 1994, 1387–1388.
4 Y. Wei, D. Jin, T. Ding, W.-H. Shih, X. Liu, S. Z. D. Cheng and Q. Fu, *Adv. Mater.*, 1998, **10**, 313–316.
5 F. Schüth, *Chem. Mater.*, 2001, **13**, 3184–3195.
6 M. H. Youn, J. G. Seo, K. M. Cho, S. Park, D. R. Park, J. C. Jung and I. K. Song, *Int. J. Hydrogen Energy*, 2008, **33**, 5052–5059.
7 M. H. Youn, J. G. Seo, J. C. Jung, S. Park, D. R. Park, S.-B. Lee and I. K. Song, *Catal. Today*, 2009, **146**, 57–62.
8 M. Benito, R. Padilla, L. Rodríguez, J. L. Sanz and L. Daza, *J. Power Sources*, 2007, **169**, 167–176.
9 H. Song and U. S. Ozkan, *Int. J. Hydrogen Energy*, 2010, **35**, 127–134.
10 P. D. Vaidya and A. E. Rodrigues, *Chem. Eng. J.*, 2006, **117**, 39–49.
11 N. Laosiripojana and S. Assabumrungrat, *Appl. Catal., B*, 2006, **66**, 29–39.
12 J.-H. Wang, C. S. Lee and M. C. Lin, *J. Phys. Chem. C*, 2009, **113**, 6681–6688.
13 A. J. Vizcaíno, A. Carrero and J. A. Calles, *Int. J. Hydrogen Energy*, 2007, **32**, 1450–1461.
14 M. H. Youn, J. G. Seo, S. Park, J. C. Jung, D. R. Park and I. K. Song, *Int. J. Hydrogen Energy*, 2008, **33**, 7457–7463.
15 D. C. Grenoble, M. M. Estadt and D. F. Ollis, *J. Catal.*, 1981, **67**, 90–102.
16 P. Biswas and D. Kunzru, *Catal. Lett.*, 2007, **118**, 36–49.
17 S. L. Lakhapatri and M. A. Abraham, *Appl. Catal., A*, 2009, **364**, 113–121.
18 S. L. Lakhapatri and M. A. Abraham, *Appl. Catal., A*, 2011, **405**, 149–159.
19 J.-Y. Zheng, J.-B. Pang, K.-Y. Qiu and Y. Wei, *Microporous Mesoporous Mater.*, 2001, **49**, 189–195.
20 M. Verónica, B. Graciela, A. Norma and L. Miguel, *Chem. Eng. J.*, 2008, **138**, 602–607.
21 W. H. R. Shaw and J. J. Bordeaux, *J. Am. Chem. Soc.*, 1955, **77**, 4729–4733.
22 S. Zeng, K. Tang, T. Li, Z. Liang, D. Wang, Y. Wang and W. Zhou, *J. Phys. Chem. C*, 2007, **111**, 10217–10225.
23 M. Déchamps, B. Djuriçić and S. Pickering, *J. Am. Ceram. Soc.*, 1995, **78**, 2873–2880.
24 F. M. Doyle and Z. Liu, *J. Colloid Interface Sci.*, 2003, **258**, 396–403.
25 K. Anoop Krishnan, K. G. Sreejalekshmi and R. S. Baiju, *Bioresour. Technol.*, 2011, **102**, 10239–10247.
26 B. N. Ryzhenko, N. I. Kovalenko, N. I. Prisyagina, N. P. Starshinova and V. V. Krupskaya, *Geochem. Int.*, 2008, **46**, 328–339.
27 G. Xu, Y. Zhang, C. Liao and C. Yan, *Solid State Commun.*, 2001, **121**, 45–49.
28 P. Biswas and D. Kunzru, *Int. J. Hydrogen Energy*, 2007, **32**, 969–980.
29 M. D. Rhodes and A. T. Bell, *J. Catal.*, 2005, **233**, 198–209.
30 J. C. Tracy, *J. Chem. Phys.*, 1972, **56**, 2736–2747.
31 R. Geyer, J. Hunold, M. Keck, P. Kraak, A. Pachulski and R. Schödel, *Chem. Ing. Tech.*, 2012, **84**, 160–164.
32 A. J. Akande, R. O. Idem and A. K. Dalai, *Appl. Catal., A*, 2005, **287**, 159–175.
33 F. Auprêtre, C. Descorme and D. Duprez, *Catal. Commun.*, 2002, **3**, 263–267.
34 J. H. Sinfelt and D. J. C. Yates, *J. Catal.*, 1967, **8**, 82–90.
35 J. Comas, F. Mariño, M. Laborde and N. Amadeo, *Chem. Eng. J.*, 2004, **98**, 61–68.
36 V. Klouz, V. Fierro, P. Denton, H. Katz, J. P. Lisse, S. Bouvot-Mauduit and C. Mirodatos, *J. Power Sources*, 2002, **105**, 26–34.
37 S. Patel and K. K. Pant, *J. Power Sources*, 2006, **159**, 139–143.
38 C.-Z. Yao, L.-C. Wang, Y.-M. Liu, G.-S. Wu, Y. Cao, W.-L. Dai, H.-Y. He and K.-N. Fan, *Appl. Catal., A*, 2006, **297**, 151–158.
39 M. H. Youn, J. G. Seo, P. Kim, J. J. Kim, H.-I. Lee and I. K. Song, *J. Power Sources*, 2006, **162**, 1270–1274.
40 T.-J. Huang and S.-Y. Jhao, *Appl. Catal., A*, 2006, **302**, 325–332.

